

A General 3D Geometry-Based Stochastic Channel Model for B5G mmWave IIoT

Wen Gu, Yang Liu*, Cheng-Xiang Wang*, *Fellow, IEEE*, Wenchao Xu, Yu Yu, Wen-Jun Lu, *Senior Member, IEEE* and Hong-Bo Zhu

Abstract—The Industrial Internet of things (IIoT) is one of the typical application scenarios in the beyond fifth generation (B5G) wireless communication systems. Due to numerous metal obstacles and machines, the industrial channel, especially at the millimeter-wave (mmWave) bands, exhibits complex characteristics that haven't been considered in existing literature. This paper proposes an innovative three-dimensional (3D) non-stationary geometry-based stochastic model (GBSM) for IIoT scenarios at mmWave bands. In the proposed model, device reflections (DR) caused by massive metal machines are modeled based on geometrical optics. Furthermore, the generalized extreme value (GEV) distribution and generalized Pareto (GP) distribution are used to parameterize the number of clusters and rays within a cluster, respectively. Further, the Doppler shift is modeled and analyzed using the Gaussian distribution. Some channel statistical characteristics are captured by the proposed model, such as the power delay profile, root-mean-square delay spread, root-

mean-square angle spread, inter-cluster delay, and space-time-frequency correlation function. Then, these channel statistical characteristics are well fitted to the ray-tracing simulations and the channel measurements. The excellent fitting results demonstrate the high accuracy of the proposed model, which is crucial for future IIoT communication system design. Whats more, this paper shows the antenna height and propagation scenarios can significantly affect the DR ratio, which should adapt to various IIoT communication scenarios.

Index Terms—IIoT, GBSM, DR, Scatter distribution, Doppler shift.

I. INTRODUCTION

AFTER the fifth generation (5G) entered the commercial deployment, international scholars and standards organizations carried out the research on the next generation communication systems to provide users with a more intelligent experience [1]. The Industrial Internet of things (IIoT) is one of the important scenarios in the beyond 5G (B5G) wireless communications. In IIoT scenarios, the production efficiency can be significantly improved through cooperative control and information interaction between multi-source heterogeneous devices. Ultra-reliable low-latency communications (uRLLC) and massive machine-type communications (mMTC) provide useful foundations for the IIoT applications [2], [3]. The millimeter-wave (mmWave) technique is applied to ensure the uRLLC and mMTC. Compared with sub-6GHz, mmWave has shorter wavelength, which can improve the efficiency of antenna. In addition, mmWave has a wide spectrum and strong anti-interference performance, which can ensure the quality of signal transmission. Therefore, mmWave is widely used in the Internet of Things, such as smart cities, wearable devices, telehealth, online education, and security systems. However, there are many types of IIoT compared with other scenarios, such as workshops, warehouses and laboratories. There are some characteristics for IIoT channels, including rich scatters, multi-mobility and high density. It is challenging to establish a general channel model for IIoT environments due to the complex channel fading patterns. Thus, it is necessary to study the characteristics of the IIoT channel in order to build an accurate channel model.

Research on the propagation channels in industrial environments can be traced back to 1988 [4], [5]. In the past decades, properties of the industrial channels have been intensively modeled. Generally, these models can be summarized into three types. The first type includes deterministic models. Based on the electromagnetic theory, deterministic models

This work was supported by the National Natural Science Foundation of China (NSFC) under Grant 61960206006, the Key Technologies R&D Program of Jiangsu (Prospective and Key Technologies for Industry) under Grants BE2022067, BE2022067-1, and BE2022067-2, the Key R&D Project of Jiangsu Province (Modern Agriculture) under Grant BE2022322, in part by the 111 Project under Grant B12018, in part by the Six talent peaks project in Jiangsu Province, in part by the open foundation of Key Laboratory of Wireless Sensor Network and Communication, Shanghai Institute of Microsystem and Information Technology, Chinese Academy of Sciences under Grant 20190917, and in part by the open research fund of Key Lab of Broadband Wireless Communication and Sensor Network Technology (Nanjing University of Posts and Telecommunications, Ministry of Education). (*Corresponding author: Yang Liu and Cheng-Xiang Wang.*)

W. Gu and Y. Liu are with the School of Internet of Things Engineering, Jiangnan University, Wuxi 214122, China, and also with the Key Lab of Broadband Wireless Communication and Sensor Network Technology (Nanjing University of Posts and Telecommunications, Ministry of Education), Nanjing 210023, China (E-mail: guwen1217@163.com and ly71354@163.com).

C.-X. Wang is with the National Mobile Communications Research Laboratory, School of Information Science and Engineering, Southeast University, Nanjing 211189, China, and also with the Purple Mountain Laboratories, Nanjing 211111, China (E-mail: chxwang@seu.edu.cn).

W. Xu is with the Department of Computing, the Hong Kong Polytechnic University, Hong Kong, China (E-mail: wenchao.xu@polyu.edu.hk).

Y. Yu is with the School of Information and Communication Engineering, Nanjing Institute of Technology, Hongjing Avenue 1, Nanjing 211167, China, and also with the Key Laboratory of Wireless Sensor Network & Communication, Shanghai Institute of Microsystem and Information Technology, Chinese Academy of Sciences, 865 Changning Road, Shanghai 200050, China (E-mail: yuyu@njit.edu.cn).

W.-J. Lu and H.-B. Zhu are with Department of Jiangsu Key Laboratory of Wireless Communications, Nanjing University of Posts and Telecommunications, Xinmofan Road 66, Nanjing 210003, China, and also with the Key Laboratory of Wireless Sensor Network & Communication, Shanghai Institute of Microsystem and Information Technology, Chinese Academy of Sciences, 865 Changning Road, Shanghai 200050, China (E-mail: wjlw@njupt.edu.cn and zhb@njupt.edu.cn).

Copyright (c) 20xx IEEE. Personal use of this material is permitted. However, permission to use this material for any other purposes must be obtained from the IEEE by sending a request to pubs-permissions@ieee.org.

Manuscript received October 13, 2022.

can accurately describe the propagation characteristics for a specific environment. However, the computational complexity is relatively high [6]. The second type includes statistical models. The key channel parameters such as path loss (PL), delay spread (DS), and angle spread (AS) are estimated to study the channel characteristics [7]. But, the universality of these models is limited in many industrial applications. The third type includes semi-statistical and semi-deterministic models. The geometry-based stochastic model (GBSM) is one of the semi-statistical and semi-deterministic models. GBSM assumes that the propagation channel is simulated by clusters, and these clusters follow the several typical distributions. Then, the channel impulse response (CIR) is obtained by using the geometrical optics theory. Compared with the deterministic and statistical models, the GBSM require lower computations and possess better generality [8]. These models have been widely used in many industrial applications. Accordingly, the GBSM is used to model the industrial channels in this paper.

However, there are still several channel properties that have not been fully considered in the existing models. For instance, the machines in industrial environments may reflect signals strongly [9], [10], but their specular reflected paths, called device reflections (DR) in this paper, have not been included and considered. Furthermore, the traditional distributions (i.e., Poisson and Gaussian distributions) cannot model the dense and random scatters in IIoT scenarios accurately. Finally, although the Doppler shift caused by movements has been considered, the fluctuations due to machine rotations in industrial scenarios have not been fully involved in GBSM [11].

To the best of the authors knowledge, there has been no general model considering the above properties of IIoT channels, such as the DR, metallic dense scatters, and oscillations of equipment. To fill this gap, a novel GBSM for IIoT scenarios is proposed in this paper. The main contributions of this paper can be summarized as follows.

- 1) Compared with the existing ones, the DR components are taken into account in the proposed mmWave-based model under the IIoT environments. Due to the high delay resolution at mmWave bands, the DR components can be resolvable in the delay domain. Both the DR and ground reflection (GR) components are modeled based on the geometrical optics of specular reflection. The effects of the antenna height and communication scenarios on the DR are also analyzed. The RT results have shown that the existence of DR components, and the DR model is accurate.

- 2) Owing to the short wavelength at mmWave bands and dense scatters in the IIoT scenarios, the generalized extreme value (GEV) and generalized Pareto (GP) distributions, instead of the Poisson distribution, are used to model the number of dense clusters and rich rays within a cluster in the industrial environments, respectively. Measurement results have shown that these distributed models are more accurate than the traditional Poisson and Gaussian ones.

- 3) Gaussian distribution is used to simulate the random Doppler shift caused by the oscillations of automated vehicles, robotic arms, and other equipment in industrial scenarios. The results have shown that the proposed Doppler shift model based on the Gaussian distribution fits well with the RT results.

The rest of this paper is organized as follows. Section II reviews the related works on industrial channel model. Section III presents the proposed GBSM in IIoT environments. Section IV explains the statistical characteristics based on the proposed model. Section V presents the simulation and verification results. Finally, Section VI concludes the paper and presents future work directions.

II. RELATED WORKS

A. Deterministic Models

The applications of deterministic models in the design of wireless sensor networks were described in [6], [12]. Several deterministic channel models based on three-dimensional (3D) ray-tracing (RT) methods were proposed for warehouse and logistic plants in [13], [14]. The propagation characteristics at different bands were further studied using the RT methods in [9]. Given the tight wireless spectrum, the communications at mmWave bands were analyzed in [15], [16], and the channel characteristics at 28 GHz and 60 GHz were examined. In addition to the RT methods, the finite-difference time-domain (FDTD) was another deterministic method for industrial channel modeling [17], [18]. The above-mentioned studies showed that the density and deployment of machine terminals have a significant effect on signal propagation in industrial environments. Generally, both the RT and FDTD deterministic models can accurately describe the propagation characteristics of an electromagnetic wave in the industrial environments.

B. Statistical Models

The Saleh-Valenzuela (SV) statistical model [7] was used to study the CIR in industrial environments in [19]–[22]. The authors of [23]–[25] focused on large-scale parameters (LSPs), including the PL, DS, and AS. These parameters were found to be modeled by log-normal, Rician, or Rayleigh distributions. The theoretical conclusions were supported by extensive measurements performed in a number of factories [26], [27]. Some typical small-scale parameters (SSPs), including power delay profile (PDP) and amplitude fading, were studied in [28]–[31]. The Rayleigh and Normal distributions were used to model the SSPs. Moreover, a few other studies paid attention to the effects of environmental factors on channel parameters. For instance, the effects of carrier frequencies on the PL and signal envelope were studied in [32], [33]. The effects of antenna distance, height, and orientation on the PL and DS were examined in [10], [34]. Although the above-mentioned studies completed the relevant analyses of industrial channel characteristics from different perspectives, they were mainly focused on the sub-6 GHz bands. Recently, the mmWave technology was applied to the IIoT field. The industrial channels were analyzed in [35]–[37], and the PL, DS, and AS models at 28 GHz – 30 GHz were developed. In [38], the number, amplitude, and delay of clusters were examined in several industrial environments at the 60 GHz. In summary, the statistical model has been used to describe the properties of industrial channel parameters.

TABLE I
DEFINITION OF KEY PARAMETERS

Parameters	Definition
$\phi_{qp,L}^{AOA}(t), \phi_{qp,L}^{EOA}(t)$	Azimuth and elevation angles of the line of sight (LOS) path from Ant_q^R to Ant_p^T
$\varphi_{qp,L}^{AOD}(t), \varphi_{qp,L}^{EOD}(t)$	Azimuth and elevation angles of the LOS path from Ant_p^T to Ant_q^R
$\phi_n^{AOA}(t), \phi_n^{EOA}(t)$	Azimuth and elevation angles between Cluster _n and the receive array center
$\varphi_n^{AOD}(t), \varphi_n^{EOD}(t)$	Azimuth and elevation angles between Cluster _n and the transmit array center
$\phi_{n,m_n}^{AOA}(t), \phi_{n,m_n}^{EOA}(t)$	Azimuth and elevation angles between m_n th ray of Cluster _n and the receive array center
$\varphi_{n,m_n}^{AOD}(t), \varphi_{n,m_n}^{EOD}(t)$	Azimuth and elevation angles between m_n th ray of Cluster _n and the transmit array center
$\phi_{GR}^{AOA}(t), \phi_{GR}^{EOA}(t)$	Azimuth and elevation angles of arrival of the GR
$\varphi_{GR}^{AOD}(t), \varphi_{GR}^{EOD}(t)$	Azimuth and elevation angles of departure of the GR
$\phi_{DR_l}^{AOA}(t), \phi_{DR_l}^{EOA}(t)$	Azimuth and elevation angles of arrival of the l th DR path
$\varphi_{DR_l}^{AOD}(t), \varphi_{DR_l}^{EOD}(t)$	Azimuth and elevation angles of departure of the l th DR path
$\mathbf{A}_q^R(t), \mathbf{A}_p^T(t)$	3D position vectors of Ant_q^R and Ant_p^T
$\mathbf{D}_n^R(t), \mathbf{D}_n^T(t)$	3D distance vectors between Cluster _n and the receive (transmit) array center
$\mathbf{D}_{n,m_n}^R(t), \mathbf{D}_{n,m_n}^T(t)$	3D distance vectors between m_n th ray of Cluster _n and the receive (transmit) array center
$\mathbf{D}_{q,m_n}^R(t), \mathbf{D}_{p,m_n}^T(t)$	3D distance vectors between m_n th ray of Cluster _n and the Ant_q^R (Ant_p^T) antenna element
$\mathbf{D}_{qp}^{LOS}(t)$	3D distance vector of the LOS components between Ant_q^R and Ant_p^T
\mathbf{D}	3D position vector of receive array center
$\mathbf{v}^R, \mathbf{v}^T, \mathbf{v}^C$	Velocity vectors of Rx, Tx and cluster _n
$\mathbf{r}_{rx,LOS}(t), \mathbf{r}_{tx,LOS}(t)$	Spherical unit vectors associated with azimuth $\phi_{qp,L}^{AOA}(t)$ ($\varphi_{qp,L}^{AOD}(t)$) and elevation $\phi_{qp,L}^{EOA}(t)$ ($\varphi_{qp,L}^{EOD}(t)$)
$\mathbf{r}_{rx,m_n}(t), \mathbf{r}_{tx,m_n}(t)$	Spherical unit vectors associated with azimuth $\phi_{n,m_n}^{AOA}(t)$ ($\varphi_{n,m_n}^{AOD}(t)$) and elevation $\phi_{n,m_n}^{EOA}(t)$ ($\varphi_{n,m_n}^{EOD}(t)$)
$\mathbf{r}_{rx,GR}(t), \mathbf{r}_{tx,GR}(t)$	Spherical unit vectors associated with azimuth $\phi_{GR}^{AOA}(t)$ ($\varphi_{GR}^{AOD}(t)$) and elevation $\phi_{GR}^{EOA}(t)$ ($\varphi_{GR}^{EOD}(t)$)
$\mathbf{r}_{rx,DR_l}(t), \mathbf{r}_{tx,DR_l}(t)$	Spherical unit vectors associated with azimuth $\phi_{DR_l}^{AOA}(t)$ ($\varphi_{DR_l}^{AOD}(t)$) and elevation $\phi_{DR_l}^{EOA}(t)$ ($\varphi_{DR_l}^{EOD}(t)$)

C. Semi-statistical and Semi-deterministic Models

In the past decades, the application of industrial scenarios has been considered in a number of standard GBSMs. The European Cooperation in the field of Scientific and Technical Research (COST) 2100 [39] and Wireless World Initiative New Radio II (WINNER II) [40] are two common 3D channel models. However, they have certain limitations in industrial mmWave communication tasks. To enhance the performance of the transmission efficiency further, massive multi-input multi-output (MIMO) and mmWave technology have been exploited in industrial networks. The International Mobile Telecommunication-2020 (IMT-2020) channel model [41] was proposed. The model has been applied only for single-mobility tasks in industrial scenarios. Then, the Quasi Deterministic Radio Channel Generation (QuaDRiGa) channel model [42] and the 3rd Generation Partnership Project TR 38.901 (3GPP TR 38.901) model [43] were defined to meet the growing demand for communications. Compared with the IMT-2020 model, QuaDRiGa and 3GPP TR 38.901 support more application scenarios, including dual-mobility scenarios. Furthermore, these models consider spatial consistency but not non-stationary property. In addition to the above-mentioned standard organizations, several research groups have studied channel properties in industrial environments. Two general 3D non-stationary GBSMs were proposed to describe the spatial non-stationary property of industrial scenarios in [44], [45]. The dense and specular multi-path components of the CIR

model in industrial environments were introduced in [46], [47]. Moreover, a GBSM for the IIoT broadband channels was proposed in [48], considering the parameters' frequency correlations. A pervasive channel model (PCM) for the sixth generation based on the GBSM is proposed in [49], which covers all the spectrum from sub-6GHz to the visible light communication bands and can be applied to a variety of scenarios, including IIoT, (ultra-)massive MIMO, and high speed train. The considerable achievements have been made in the research of constructing industrial channel model based on GBSM.

III. A NON-STATIONARY IIoT 3D GBSM MODEL

This paper presents an $M_R \times M_T$ IIoT communication system at the mmWave bands. Assume that M_T and M_R denote the number of antennas at the transmitter (Tx) and receiver (Rx) sides, respectively. A two-bounce propagation mechanism is employed in the proposed model. The scattering environments between the Tx and Rx are modeled as effective clusters. Let $Cluster_n$ represents n th cluster. $Cluster_n$ is consisted by a pair of sub-clusters, namely, the first-bounce from Tx to the $Cluster_n^F$, the last-bounce from $Cluster_n^L$ to Rx, and the virtual link between the first-bounce and last-bounce. The proposed GBSM model is shown in Fig. 1, where Ant_p^T denotes a transmitting antenna p , and Ant_q^R is a receiving antenna q . The other parameters are listed in Table I.

Moreover, $h_{rx,q}$ and $h_{tx,p}$ is the height of Ant_q^R and Ant_p^T , respectively. $d_{l,qp}(t)$ is the distance between the projections of Ant_q^R and Ant_p^T onto the l th reflective surface. These distances can be calculated from the spatial geometric relationships.

As shown in Fig. 3, the delay and angle of the DR components can be expressed as

$$d_{qp,l}^{DR}(t) = \sqrt{(d_{l,q}(t) + d_{l,p}(t))^2 + (h_{rx,q}(t) - h_{tx,p}(t))^2 + d_{l,qp}^2(t)} \quad (8)$$

$$\tau_{qp,l}^{DR}(t) = \frac{d_{qp,l}^{DR}(t)}{c} \quad (9)$$

$$\varphi_{DR_i}^{EOD}(t) = \phi_{DR_i}^{EOA}(t) = \text{acr tan} \left(\frac{d_{l,q}(t) + d_{l,p}(t)}{h_{rx,q}(t) - h_{tx,p}(t)} \right) \quad (10)$$

$$\varphi_{DR_i}^{AOD}(t) = \varphi_{qp,L}^{AOD}(t) \quad (11)$$

$$\phi_{DR_i}^{AOA}(t) = \varphi_{DR_i}^{AOD}(t) + 180^\circ. \quad (12)$$

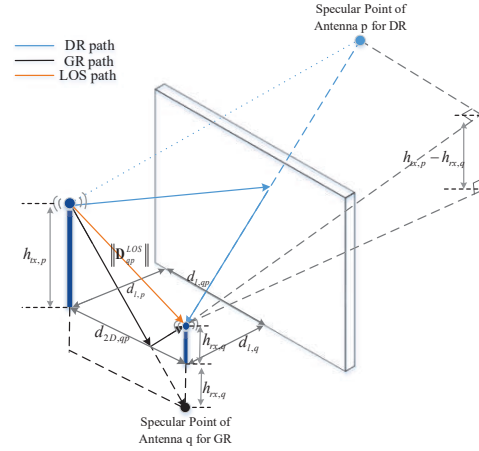


Fig. 3. Geometric principles of the DR components.

The power of the l th DR path is assumed to be proportional

$$h_{qp}(t, \tau) = \sqrt{\frac{K}{K+1}} \left(h_{qp}^{LOS}(t) \delta(\tau - \tau_{qp}^{LOS}(t)) + h_{qp}^{GR}(t) \delta(\tau - \tau_{qp}^{GR}(t)) + \sum_{l=1}^{L(t)} h_{qp,l}^{DR}(t) \delta(\tau - \tau_{qp,l}^{DR}(t)) \right) + \sqrt{\frac{1}{K+1}} \left(\sum_{n=1}^{N(t)} \sum_{m_n=1}^{M_n(t)} h_{qp,n,m_n}^{NLOS}(t) \delta(\tau - \tau_{n,m_n}(t)) \right) \quad (1)$$

$$h_{qp}^{LOS}(t) = \begin{bmatrix} F_{q,V}^T(\varphi_{qp,L}^{AOD}(t), \varphi_{qp,L}^{EOD}(t)) \\ F_{q,H}^T(\varphi_{qp,L}^{AOD}(t), \varphi_{qp,L}^{EOD}(t)) \end{bmatrix}^T \begin{bmatrix} e^{j\Phi_{LOS}} & 0 \\ 0 & -e^{j\Phi_{LOS}} \end{bmatrix} \begin{bmatrix} F_{q,V}^R(\phi_{qp,L}^{AOA}(t), \phi_{qp,L}^{EOA}(t)) \\ F_{q,H}^R(\phi_{qp,L}^{AOA}(t), \phi_{qp,L}^{EOA}(t)) \end{bmatrix} \exp \left(j2\pi \frac{1}{\lambda} \left(-\|\mathbf{D}_{qp}^{LOS}\| + \mathbf{r}_{rx,LOS}^T(t) \cdot \mathbf{A}_q^R(t) + \mathbf{r}_{tx,LOS}^T(t) \cdot \mathbf{A}_p^T(t) + f_{LOS}^{doppler}(t) \cdot t \right) \right) \quad (2)$$

$$h_{qp,n,m_n}^{NLOS}(t) = \begin{bmatrix} F_{q,V}^T(\varphi_{n,m_n}^{EOD}(t), \varphi_{n,m_n}^{AOD}(t)) \\ F_{q,H}^T(\varphi_{n,m_n}^{EOD}(t), \varphi_{n,m_n}^{AOD}(t)) \end{bmatrix}^T \begin{bmatrix} e^{j\Phi_{n,m_n}^{VV}} & \sqrt{\kappa} e^{j\Phi_{n,m_n}^{VH}} \\ \sqrt{\kappa} e^{j\Phi_{n,m_n}^{HV}} & e^{j\Phi_{n,m_n}^{HH}} \end{bmatrix} \begin{bmatrix} F_{q,V}^R(\phi_{n,m_n}^{EOA}(t), \phi_{n,m_n}^{AOA}(t)) \\ F_{q,H}^R(\phi_{n,m_n}^{EOA}(t), \phi_{n,m_n}^{AOA}(t)) \end{bmatrix} \sqrt{P_{n,m_n}(t)} \exp \left(j2\pi \frac{1}{\lambda} \left(\mathbf{r}_{rx,m_n}^T(t) \cdot \mathbf{A}_q^R(t) + \mathbf{r}_{tx,m_n}^T(t) \cdot \mathbf{A}_p^T(t) + f_{m_n}^{doppler}(t) \cdot t \right) \right) \quad (3)$$

$$h_{qp}^{GR}(t) = \frac{\|\mathbf{D}_{qp}^{LOS}(t)\|}{d_{qp}^{GR}(t)} \begin{bmatrix} F_{q,V}^T(\varphi_{GR}^{EOD}(t), \varphi_{GR}^{AOD}(t)) \\ F_{q,H}^T(\varphi_{GR}^{EOD}(t), \varphi_{GR}^{AOD}(t)) \end{bmatrix}^T \begin{bmatrix} R_{||}^{GR}(t) & 0 \\ 0 & -R_{\perp}^{GR}(t) \end{bmatrix} \begin{bmatrix} F_{q,V}^R(\phi_{GR}^{EOA}(t), \phi_{GR}^{AOA}(t)) \\ F_{q,H}^R(\phi_{GR}^{EOA}(t), \phi_{GR}^{AOA}(t)) \end{bmatrix} \exp \left(j2\pi \frac{1}{\lambda} \left(\mathbf{r}_{rx,GR}^T(t) \cdot \mathbf{A}_q^R(t) + \mathbf{r}_{tx,GR}^T(t) \cdot \mathbf{A}_p^T(t) + f_{GR}^{doppler}(t) \cdot t \right) \right) \quad (4)$$

$$h_{qp,l}^{DR}(t) = \frac{\|\mathbf{D}_{qp}^{LOS}(t)\|}{d_{qp,l}^{DR}(t)} \begin{bmatrix} F_{q,V}^T(\varphi_{DR_i}^{EOD}(t), \varphi_{DR_i}^{AOD}(t)) \\ F_{q,H}^T(\varphi_{DR_i}^{EOD}(t), \varphi_{DR_i}^{AOD}(t)) \end{bmatrix}^T \begin{bmatrix} R_{||}^{DR_i}(t) & 0 \\ 0 & -R_{\perp}^{DR_i}(t) \end{bmatrix} \begin{bmatrix} F_{q,V}^R(\phi_{DR_i}^{EOA}(t), \phi_{DR_i}^{AOA}(t)) \\ F_{q,H}^R(\phi_{DR_i}^{EOA}(t), \phi_{DR_i}^{AOA}(t)) \end{bmatrix} \exp \left(j2\pi \frac{1}{\lambda} \left(\mathbf{r}_{rx,DR_i}^T(t) \cdot \mathbf{A}_q^R(t) + \mathbf{r}_{tx,DR_i}^T(t) \cdot \mathbf{A}_p^T(t) + f_{DR_i}^{doppler}(t) \cdot t \right) \right) \quad (5)$$

to the LOS path power $P_{qp}^{LOS}(t)$. The power of the l th DR path is calculated as

$$P_{qp,l}^{DR}(t) = \left(\frac{\|\mathbf{D}_{LOS}(t)\|}{d_{qp,l}^{DR}(t)} \right)^2 \cdot P_{qp}^{LOS}(t). \quad (13)$$

The above parameters about the LOS components will be given in Section II-E. Similar to the DR components, the angle and delay of GR components are determined as

$$d_{qp}^{GR}(t) = \sqrt{(h_{tx,p}(t) + h_{rx,q}(t))^2 + d_{2D,qp}^2(t)} \quad (14)$$

$$\tau_{qp}^{GR}(t) = \frac{d_{qp}^{GR}(t)}{c} \quad (15)$$

$$\begin{aligned} \varphi_{GR}^{EOD}(t) &= \phi_{GR}^{EOA}(t) \\ &= 180^\circ - \text{acr} \tan \left(\frac{d_{2D,qp}(t)}{h_{rx,q}(t) + h_{tx,p}(t)} \right) \end{aligned} \quad (16)$$

$$\varphi_{GR}^{AOD}(t) = \varphi_{qp,L}^{AOD}(t) \quad (17)$$

$$\phi_{GR}^{AOA}(t) = \varphi_{GR}^{AOD}(t) + 180^\circ \quad (18)$$

where $d_{2D,qp}(t)$ is the horizontal distance between Ant_q^R and Ant_p^T . Then, the GR power is calculated as

$$P_{qp}^{GR}(t) = \left(\frac{\|\mathbf{D}_{LOS}(t)\|}{d_{qp}^{GR}(t)} \right)^2 \cdot P_{qp}^{LOS}(t). \quad (19)$$

The relationship between K_{GR} , K_{DR} , and K_{LOS} can be obtained from (13) and (19), i.e., $K_{GR} = \left(\frac{\|\mathbf{D}_{LOS}(t)\|}{d_{qp}^{GR}(t)} \right)^2 \cdot K_{LOS}$ and $K_{GR} = \sum_{l=1}^{L(t)} \left(\frac{\|\mathbf{D}_{LOS}(t)\|}{d_{qp,l}^{GR}(t)} \right)^2 \cdot K_{LOS}$.

C. Numbers of Clusters and Rays within Cluster_n

In traditional methods, Poisson or Gaussian distribution is commonly used to simulate the number of clusters and rays within a cluster. However, industrial channels show rich scatters and high density. Therefore, these models cannot describe the number of clusters and rays within a cluster accurately in industrial environments. The extensive measurement results show that the GEV and GP distributions can be used to simulate the number of clusters and rays within a cluster in industrial environments [38].

The GEV distribution indicates the probability distribution of extreme values in random variables following independent and identically distributed (i.i.d). The number of clusters $N(t)$ follows the GEV distribution, which is given as $N(t) \sim GEV(k_e, \sigma_e, \mu_e)$. The distribution function of the GEV distribution [50] is calculated as

$$P_{GEV}(N(t)) = \exp \left(- \left[1 + k_e \left(\frac{N(t) - \mu_e}{\sigma_e} \right) \right]^{-\frac{1}{k_e}} \right). \quad (20)$$

The PDF is expressed as

$$\begin{aligned} g_{GEV}(N(t)) &= \frac{1}{\sigma_e} \left[1 + \frac{\sigma_e (N(t) - \mu_e)}{k_e} \right]^{-(1+k_e^{-1})} \\ &\cdot \exp \left\{ - \left[1 + \frac{k_e (N(t) - \mu_e)}{\sigma_e} \right]^{-k_e^{-1}} \right\} \end{aligned} \quad (21)$$

where k_e and μ_e denote the shape parameter and position parameter, respectively. $\sigma_e > 0$ is the scale parameter. k_e determines the distribution type. $k_e = 0$, $k_e > 0$, and $k_e < 0$ represent the Gumbel extreme value distribution, Frechet extreme value distribution, and Weibull extreme value distribution, respectively. μ_e determines the minimum of the distribution variable, and the larger μ_e leads to the larger minimum of $N(t)$. σ_e determines the span of tail of the distribution, and the larger σ_e leads to the larger span of $N(t)$.

The GP distribution describes the probability distribution of excess quantities in random variables following i.i.d. The number of rays within a cluster $M_n(t)$ is assumed to follow the GP distributed, i.e., $M_n(t) \sim GP(k_p, \sigma_p, \mu_p)$. The distribution function of the GP distribution [51] is given as

$$P_{GP}(M_n(t)) = 1 - \left(1 + k_p \frac{M_n(t) - \mu_p}{\sigma_p} \right)^{-\frac{1}{k_p}}. \quad (22)$$

The PDF is expressed as

$$g_{GP}(M_n(t)) = \frac{1}{\sigma_p} \left(1 + k_p \frac{M_n(t) - \mu_p}{\sigma_p} \right)^{-\frac{1}{k_p}-1} \quad (23)$$

where k_p and μ_p represent the shape parameter and position parameter, respectively. $\sigma_p > 0$ is the scale parameter. k_p determines the distribution type. $k_p = 0$, $k_p > 0$, and $k_p < 0$ represent the Pareto I distribution, Pareto II distribution, and Pareto III distribution, respectively. μ_p determines the minimum of the distribution variable, and the larger μ_p leads to the larger minimum of $M_n(t)$. σ_p determines the span of tail of the distribution, and the larger σ_p leads to the larger span of $M_n(t)$.

D. Doppler Shift Modeling

For the deterministic components, the Doppler shift is defined as

$$f_x^{doppler}(t) = \frac{\mathbf{r}_{rx,X}^T(t) \cdot \mathbf{v}^R(t) + \mathbf{r}_{tx,X}^T(t) \cdot \mathbf{v}^T(t)}{\lambda_c} \quad (24)$$

where the subscript $x = \{\text{LOS, GR, DR}_l\}$ represents the LOS, GR, or the l th DR component.

Previous research [11] showed that the oscillations of machine generate random Doppler offsets. Therefore, the Doppler shift in industrial environments can be obtained from the traditional Doppler shift plus a random frequency offset for NLOS components, and is defined as

$$f_{m_n}^{doppler}(t) = \frac{\mathbf{r}_{rx,m_n}^T(t) \cdot \mathbf{v}^R(t) + \mathbf{r}_{tx,m_n}^T(t) \cdot \mathbf{v}^T(t)}{\lambda_c} + \Delta f \quad (25)$$

where Δf is the random Doppler frequency offset, which follows the Gaussian distribution with the zero mean and σ_f standard deviation, i.e., $\Delta f \sim N(0, \sigma_f)$.

E. Generation of other Parameters

The generation of other parameters involved in the proposed model will be listed in the following.

1) *Generation of Angle*: Angles $\phi_n^{AOA}(t)$, $\phi_n^{EOA}(t)$, $\varphi_n^{AOD}(t)$, and $\varphi_n^{EOD}(t)$ of $Cluster_n$ follow the wrapped Gaussian distribution. Then, the angles of m_n th ray are obtained by the angles of $Cluster_n$ plus the angle deviations [45], can be expressed as

$$\begin{bmatrix} \phi_{n,m_n}^{AOA}(t) & \phi_{n,m_n}^{EOA}(t) & \varphi_{n,m_n}^{AOD}(t) & \varphi_{n,m_n}^{EOD}(t) \\ \phi_n^{AOA}(t) & \phi_n^{EOA}(t) & \varphi_n^{AOD}(t) & \varphi_n^{EOD}(t) \end{bmatrix} + \begin{bmatrix} \Delta\phi_{m_n}^{AOA} & \Delta\phi_{m_n}^{EOA} & \Delta\varphi_{m_n}^{AOD} & \Delta\varphi_{m_n}^{EOD} \end{bmatrix} = \quad (26)$$

where $\Delta\phi_{m_n}^{AOA}$, $\Delta\phi_{m_n}^{EOA}$, $\Delta\varphi_{m_n}^{AOD}$, and $\Delta\varphi_{m_n}^{EOD}$ are the random angular offsets of the ray and follow the Laplace distribution with the zero mean and standard deviation of 1 degree. It is worth noting that the standard deviation of angular offsets can be modified by measurements.

From the above parameters, the distance vectors $\mathbf{D}_n^T(t)$ and $\mathbf{D}_n^R(t)$ of $Cluster_n$ on the Tx and Rx sides can be respectively obtained as

$$\mathbf{D}_n^R(t) = D_n^R(t) \begin{bmatrix} \cos \phi_n^{EOA}(t) \cos \phi_n^{AOA}(t) \\ \cos \phi_n^{EOA}(t) \sin \phi_n^{AOA}(t) \\ \sin \phi_n^{EOA}(t) \end{bmatrix} + \mathbf{D} \quad (27)$$

$$\mathbf{D}_n^T(t) = D_n^T(t) \begin{bmatrix} \cos \varphi_n^{EOD}(t) \cos \varphi_n^{AOD}(t) \\ \cos \varphi_n^{EOD}(t) \sin \varphi_n^{AOD}(t) \\ \sin \varphi_n^{EOD}(t) \end{bmatrix} \quad (28)$$

where $D_n^T(t)$ and $D_n^R(t)$ are the Frobenius norms of $\mathbf{D}_n^T(t)$ and $\mathbf{D}_n^R(t)$, respectively, and they follow exponential distribution. Similarly, $\mathbf{D}_{n,m_n}^T(t)$ and $\mathbf{D}_{n,m_n}^R(t)$ can be calculated. Then, the $\mathbf{D}_{p,m_n}^T(t)$ and $\mathbf{D}_{q,m_n}^R(t)$ can be obtained as $\mathbf{D}_{p,m_n}^T(t) = \mathbf{D}_{n,m_n}^T(t) - \mathbf{A}_p^T(t)$ and $\mathbf{D}_{q,m_n}^R(t) = \mathbf{D}_{n,m_n}^R(t) - \mathbf{A}_q^R(t)$, respectively.

2) *Generation of Delay*: The delay of LOS component is given as $\tau_{qp}^{LOS}(t) = \|\mathbf{D}_{qp}^{LOS}(t)\|/c$, where $\mathbf{D}_{qp}^{LOS}(t) = \mathbf{A}_q^R(t) - \mathbf{A}_p^T(t)$ is the LOS distance vector between Ant_q^R and Ant_p^T , and c represents the speed of light.

The delay of $Cluster_n$ is expressed by $\tau_n(t)$. Then, the delays of NLOS components can be written as

$$\tau_n(t) = [\|\mathbf{D}_n^R(t)\| - \|\mathbf{D}_n^T(t)\|] / c + \tilde{\tau}(t) \quad (29)$$

$$\tau_{n,m_n}(t) = [\|\mathbf{D}_{q,m_n}^R(t)\| - \|\mathbf{D}_{p,m_n}^T(t)\|] / c + \tilde{\tau}(t) \quad (30)$$

where $\tilde{\tau}(t) = -r_\tau \sigma_\tau \ln \mu_n$ represents virtual delay. r_τ and σ_τ are the delay ratio and the delay spread factor, respectively. μ_n is a random variable that follows the uniform distribution $\mu_n \sim U(0, 1)$.

3) *Generation of Power*: The mean power of $Cluster_n$ can be calculated as [43]

$$P_n(t) = \exp\left(-\tau_n(t) \frac{r_\tau - 1}{r_\tau \sigma_\tau}\right) \cdot 10^{-\frac{Z_n}{10}} \quad (31)$$

where Z_n follows the Gaussian distribution of $Z_n \sim N(0, \sigma_n)$, and σ_n is the shadow fading standard deviation of $Cluster_n$. The mean power of the m_n th ray within $Cluster_n$ is expressed as

$$P'_{n,m_n}(t) = \exp\left(-\tau_{n,m_n}(t) \frac{r_\tau - 1}{r_\tau \sigma_\tau}\right) \cdot 10^{-\frac{Z_n}{10}} \quad (32)$$

Then, the mean power of the m_n th ray within $Cluster_n$ is proportionally scaled at the mean power of $Cluster_n$ as

$$\tilde{P}_{n,m_n}(t) = P_n(t) \frac{P'_{n,m_n}(t)}{\sum_{m_n} P'_{n,m_n}(t)}. \quad (33)$$

Equation (33) is normalized as $P_{n,m_n}(t) = \frac{\tilde{P}_{n,m_n}(t)}{\sum_{m_n} \tilde{P}_{n,m_n}(t)}$. It is worth mentioning that the LOS path power is defined as $P_{qp}^{LOS}(t) = K_{LOS}$.

F. Time-Space Non-stationary Characteristics

Due to the time-varying characteristics and the introduction of massive MIMO technologies, a B5G industrial channel exhibits time-space non-stationary characteristics. These characteristics can be described by the birth-death process of clusters on the time-array axis [45]. The generation and recombination rates of a cluster are denoted by λ_G and λ_R in this paper. Assume p' and q' are the unit antennas different from p and q at the time t , respectively. After time $t + \Delta t$, the joint survival probability of a cluster of antennas q (p) and q' (p') on the time-array axis is given as

$$P_{sur}(\Delta t, \delta_R, \delta_T) = \exp\left[-\lambda_R \left(\frac{\delta_R + \delta_T}{D_c^s} + \frac{P_F(\Delta v^R + \Delta v^T)\Delta t}{D_c^t}\right)\right] \quad (34)$$

where $\delta_R = \|\mathbf{A}_q^R - \mathbf{A}_{q'}^R\|$ is the spacing between the unit antennas q and q' in Rx array. $\delta_T = \|\mathbf{A}_p^T - \mathbf{A}_{p'}^T\|$ is the spacing between the unit antennas p and p' in Tx array. $\Delta v^R = E[\|\mathbf{v}^R - \mathbf{v}^C\|]$ and $\Delta v^T = E[\|\mathbf{v}^T - \mathbf{v}^C\|]$ indicate the mean relative velocities on the Rx and Tx sides, respectively. D_c^s and D_c^t are the scenario-relevant coefficients describing the spatial and temporal domains, respectively. P_F represents the percentage of moving clusters in an industrial environment. Based on the birth-death process, the number of new clusters for antenna $q'(p')$ is generated according to the Poisson distribution with a mean of

$$E[N_{new}] = \frac{\lambda_G}{\lambda_R} (1 - P_{sur}(\Delta t, \delta_R, \delta_T)). \quad (35)$$

Then, the new clusters will be assigned parameters. Meanwhile, the survival clusters $\mathbf{C}_q^R(t)$ and $\mathbf{C}_p^T(t)$ will be updated with geometric position, delay, and power after Δt , i.e., $\mathbf{C}_p^T(t) \xrightarrow{E} \mathbf{C}_p^T(t + \Delta t)$ and $\mathbf{C}_q^R(t) \xrightarrow{E} \mathbf{C}_q^R(t + \Delta t)$. Then, the delay and power at time $(t + \Delta t)$ are calculated based on the new geometric position, as described in Section II-E. The new distance vectors are calculated as

$$\mathbf{D}_n^T(t + \Delta t) = \mathbf{D}_n^T(t) + \mathbf{v}^T \Delta t \quad (36)$$

$$\mathbf{D}_n^R(t + \Delta t) = \mathbf{D}_n^R(t) + \mathbf{v}^R \Delta t. \quad (37)$$

IV. CHANNEL STATISTICAL CHARACTERISTICS

Channel statistical characteristics play a significant role in wireless channel model and performance analysis. Some channel statistical characteristics are studied in this paper, include the PDP, power ratio of DR components, root-mean-square DS (RMS DS), root-mean-square AS (RMS AS), inter-cluster delay, and space-time-frequency correlation function (STFCF).

A. Time-variant Power Delay Profile

The delay and power of the Tx signal varies through different paths to the Rx. PDP describes the dispersion of the channel in time. The time-variant properties of PDP are caused by the time-varying characteristics of the delay, power, and visible clusters. The PDP is calculated as

$$\begin{aligned}
 PDP(t, \tau) = & P_{qp}^{LOS}(t) \delta [\tau - \tau_{qp}^{LOS}(t)] \\
 & + P_{qp}^{GR}(t) \delta [\tau - \tau_{qp}^{GR}(t)] \\
 & + \sum_{l=1}^{L(t)} P_{qp,l}^{DR}(t) \delta [\tau - \tau_{qp,l}^{DR}(t)] \\
 & + \sum_{n=1}^{N(t)} \sum_{m_n=1}^{M_n(t)} P_{n,m_n}(t) \delta [\tau - \tau_{n,m_n}(t)]
 \end{aligned} \quad (38)$$

B. Power Ratio of DR

One of the key characteristics of this paper is the power ratio of the DR components. It is the ratio of the total power of the DR components to the total power of all components, which can be written as

$$\eta(t) = \frac{P_{DR}(t)}{P_{LOS}(t) + P_{NLOS}(t) + P_{GR}(t) + P_{DR}(t)} \quad (39)$$

where P_{GR} , P_{DR} , P_{LOS} , and P_{NLOS} are the total power of GR, DR, LOS, and NLOS components, respectively.

After normalization in Section II-E, the sum of the power of all NLOS paths is unit one. Bringing the power of each component in Section II into (39), the power ratio of DR components can be calculated as

$$\eta(t) = \frac{\sum_{l=1}^{L(t)} \left(\frac{\|\mathbf{D}_{qp}^{LOS}(t)\|}{d_{qp,l}^{DR}(t)} \right)^2 \cdot K_{LOS}}{\left(1 + \left(\frac{\|\mathbf{D}_{qp}^{LOS}(t)\|}{d_{qp}^{GR}(t)} \right)^2 + \sum_{l=1}^{L(t)} \left(\frac{\|\mathbf{D}_{qp}^{LOS}(t)\|}{d_{qp,l}^{DR}(t)} \right)^2 \right) \cdot K_{LOS} + 1} \quad (40)$$

C. Root-Mean-Square Delay Spread and Root-Mean-Square Angle Spread

The DS is the key indicator to describe the temporal dispersion of multi-path channels. It is also an important parameter to determine whether the receiver needs an adaptive equalizer or not. The RMS DS can be expressed as [27]

$$DS(t) = \sqrt{\frac{\sum P_k(t) \tau_k^2(t)}{\sum P_k(t)} - \left(\frac{\sum P_k(t) \tau_k(t)}{\sum P_k(t)} \right)^2} \quad (41)$$

where $\tau_k(t)$ and $P_k(t)$ are the delay and the power of the k th path at time t , respectively.

Similarly, the RMS AS can be calculated as

$$DS(t) = \sqrt{\frac{\sum P_k(t) \alpha_k^2(t)}{\sum P_k(t)} - \left(\frac{\sum P_k(t) \alpha_k(t)}{\sum P_k(t)} \right)^2} \quad (42)$$

where $\alpha_k(t)$ is the angle of the k^{th} path at time t .

TABLE II
GENERAL SIMULATION PARAMETERS

$\phi_{qp,L}^{AOA}(t_0)$	$\phi_{qp,L}^{EOA}(t_0)$	$\varphi_{qp,L}^{AOD}(t_0)$	$\varphi_{qp,L}^{EOD}(t_0)$	Antenna Spacing
$\frac{\pi}{4} \text{ rad}$	$\frac{\pi}{3} \text{ rad}$	$\frac{\pi}{4} \text{ rad}$	$\frac{\pi}{4} \text{ rad}$	0.5λ

TABLE III
SCENARIOS PARAMETERS OF RT.

Scenarios	Workshop	Lab	Warehouse
Length (m)	50	12	85
Wide (m)	30	7	65
Height (m)	7	7	8
Tx Height (m)	1	0.5	2.5
Rx Height (m)	0.5	1	2.5
M_R	1	1	1
M_T	1	1	1
v^T (m/s)	0.5	0	0
v^R (m/s)	0	0	0

D. Inter-cluster Delay

The properties of rich scatters in IIoT channels lead to considerable inter-cluster delay in IIoT channels. The inter-cluster delay $\Delta\tau(t)$ is defined as delay difference between two subsequent clusters, which can be expressed as

$$\Delta\tau(t) = \tau_{n'}(t) - \tau_n(t) \quad (43)$$

where $\tau_{n'}(t)$ is the delay of $Cluster_{n'}$ that is different from $Cluster_n$.

E. Space-Time-Frequency Correlation Function

The STFCCF is one of the important functions in studying the IIoT channel correlation. In this work, the time-variant transfer function $H_{qp}(t, f)$ is introduced to calculate the STFCCF. Function $H_{qp}(t, f)$ is the Fourier transform of $h_{qp}(t, \tau)$ relative to the delay τ , and can be expressed as (45), where f is frequency. Then, the STFCCF can be calculated as [52]

$$\begin{aligned}
 R_{qp,q'p'}(\delta_R, \delta_T, \Delta f, \Delta t, f, t) = \\
 E [H_{qp}(t, f) H_{q'p'}^*(t + \Delta t, f + \Delta f)]
 \end{aligned} \quad (44)$$

where $(\cdot)^*$ represents the complex conjugate operation.

In this study, it is assumed that LOS, GR, DR, and NLOS components are independent of each other for simplicity. Therefore, (44) can be further modeled as (46). Correlation functions of LOS, GR, DR, and NLOS components are written as (47) – (50), respectively, where $\sigma_{LOS} = f[\tau_{qp}^{LOS}(t) - \tau_{q'p'}^{LOS}(t + \Delta t)] + \Delta f \tau_{qp}^{LOS}(t + \Delta t)$, $\sigma_{GR} = f[\tau_{qp}^{GR}(t) - \tau_{q'p'}^{GR}(t + \Delta t)] + \Delta f \tau_{qp}^{GR}(t + \Delta t)$, $\sigma_{DR_i} = f[\tau_{qp,l}^{DR}(t) - \tau_{q'p',l}^{DR}(t + \Delta t)] + \Delta f \tau_{qp,l}^{DR}(t + \Delta t)$, and $\sigma_{NLOS} = f[\tau_{n,m_n}(t) - \tau_{n',m_{n'}}(t + \Delta t)] + \Delta f \tau_{n,m_n}(t + \Delta t)$. The STFCCF has high-dimensional complexity. However, the STFCCF can be reduced to the temporal auto-correlation function (ACF), space cross-correlation function (CCF), and frequency correlation function (FCF) by setting f , p (p'), q (q'), and t . The STFCCF can be reduced to the ACF by setting

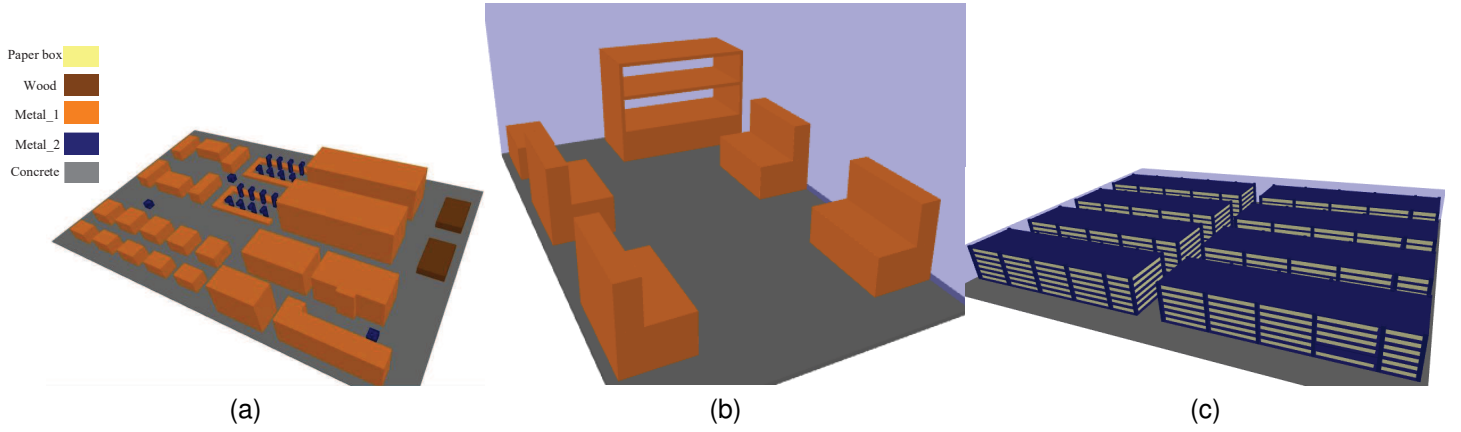


Fig. 4. Simulated B5G IIoT environments by RT: (a) Automatic Workshop, (b) Lab, and (c) Warehouse.

$\Delta f = 0$, $p = p'$, and $q = q'$. Similarly, the STFCCF can be reduced to the CCF on the Tx or Rx side by setting $\Delta f = 0$, $\Delta t = 0$, and $p = p'$ (or $q = q'$). Finally, the STFCCF can be reduced to the FCF by setting $\Delta t = 0$, $p = p'$, and $q = q'$.

V. MODEL VALIDATIONS AND ANALYSIS

The statistical properties are simulated and analyzed to validate the accuracy and validity of the proposed IIoT channel

model. The general parameters are based on parameter estimation and measurement statistics, as shown in Table II. The percentage of the moving clusters is set to $P_F = 0.3$ [53]. The other parameters will be given in the analysis description.

To analyze the necessity of considering the DR components in channel modeling, RT simulations are performed in several typical B5G IIoT scenarios, including automatic workshop, lab, and warehouse, as shown in Fig. 4. The power and gain of Tx is set to 10 dBm and 5 dBi, respectively. Different

$$\begin{aligned}
 H_{qp}(t, f) &= \int_{-\infty}^{\infty} h_{qp}(t, \tau) e^{-j2\pi f \tau} d\tau \\
 &= \sqrt{\frac{K}{K+1}} \left(h_{qp}^{LOS}(t, \tau) e^{-j2\pi f \tau_{qp}^{LOS}(t)} + h_{qp}^{GR}(t, \tau) e^{-j2\pi f \tau_{qp}^{GR}(t)} + \sum_{l=1}^{L(t)} h_{qp,l}^{DR}(t, \tau) e^{-j2\pi f \tau_{qp,l}^{DR}(t)} \right) \\
 &+ \sqrt{\frac{1}{K+1}} \sum_{n=1}^{N(t)} \sum_{m_n}^{M_n(t)} h_{qp,n,m_n}^{NLOS}(t, \tau) e^{-j2\pi f \tau_{n,m_n}(t)}
 \end{aligned} \quad (45)$$

$$\begin{aligned}
 R_{qp,q'p'}(\delta_R, \delta_T, \Delta f, \Delta t, f, t) &= R_{qp,q'p'}^{LOS}(\delta_R, \delta_T, \Delta f, \Delta t, f, t) + R_{qp,q'p'}^{GR}(\delta_R, \delta_T, \Delta f, \Delta t, f, t) \\
 &+ R_{qp,q'p'}^{DR}(\delta_R, \delta_T, \Delta f, \Delta t, f, t) + R_{qp,q'p'}^{NLOS}(\delta_R, \delta_T, \Delta f, \Delta t, f, t)
 \end{aligned} \quad (46)$$

$$R_{qp,q'p'}^{LOS}(\delta_R, \delta_T) = \frac{K^{LOS}}{K+1} h_{qp}^{LOS}(t, \tau) h_{q'p'}^{LOS}(t, \tau) e^{j2\pi \sigma_{LOS}} \quad (47)$$

$$R_{qp,q'p'}^{GR}(\delta_R, \delta_T) = \frac{K^{GR}}{K+1} h_{qp}^{GR}(t, \tau) h_{q'p'}^{GR}(t, \tau) e^{j2\pi \sigma_{GR}} \quad (48)$$

$$R_{qp,q'p'}^{DR}(\delta_R, \delta_T) = \frac{K^{DR}}{K+1} \sum_{l=1}^{L(t)} \sum_{l'=1}^{L'(t)} h_{qp,l}^{DR}(t, \tau) h_{q'p',l'}^{DR}(t, \tau) e^{j2\pi \sigma_{DR,l}} \quad (49)$$

$$R_{qp,q'p'}^{NLOS}(\delta_R, \delta_T) = \frac{P_{sur}(\Delta t, \delta_R, \delta_T)}{K+1} E \left[\sum_{n=1}^N \sum_{n'=1}^N \sum_{m_n=1}^{M_n} \sum_{m_{n'}=1}^{M_{n'}} h_{qp,n,m_n}^{NLOS}(t, \tau) h_{q'p',n',m_{n'}}^{NLOS}(t, \tau) e^{j2\pi \sigma_{NLOS}} \right] \quad (50)$$

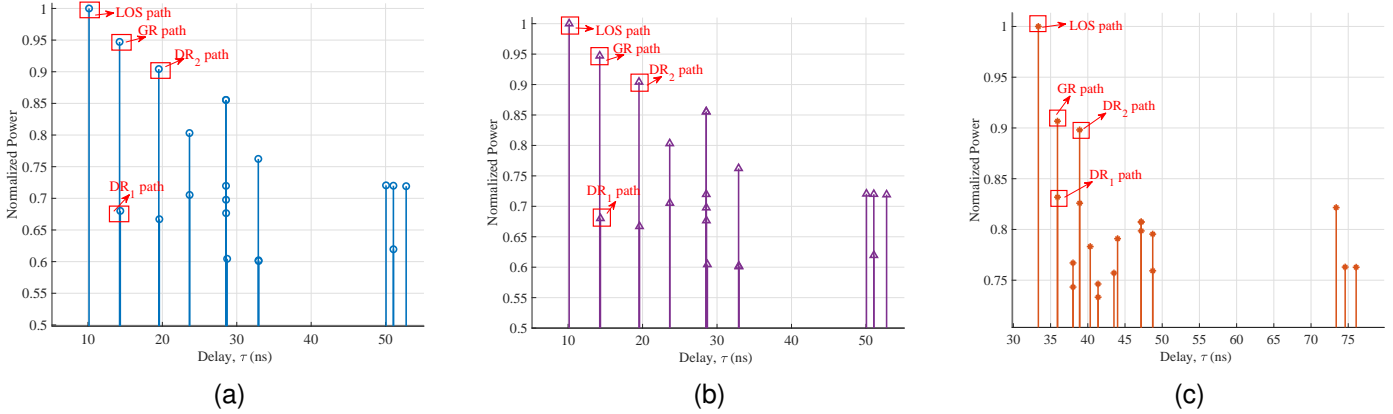


Fig. 5. PDP results of RT simulation: (a) Automatic Workshop, (b) Lab, and (c) Warehouse.

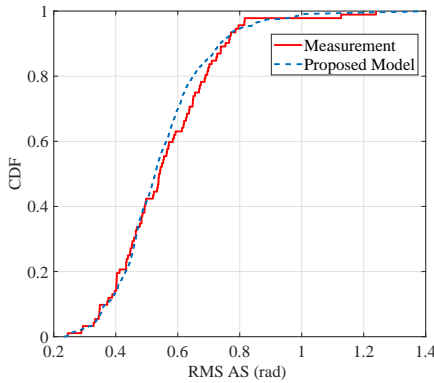


Fig. 6. The CDFs of RMS ASA of the proposed model, measurement in [56] for the IIoT scenario ($f_c = 5.5$ GHz, $M_R = 32$, $M_T = 64$, $[\text{std}(\phi_n^{AOA}), \text{std}(\phi_n^{EOD}), \text{std}(\varphi_n^{EOD})] = [35.8, 16, 20.6, 12]$).

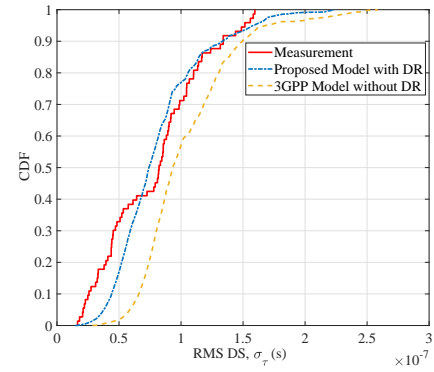


Fig. 7. The CDFs of RMS DS of the proposed model, measurement in [56] for the IIoT scenario ($f_c = 5.5$ GHz, $M_R = M_T = 1$, $D_c^s = 10$ m, $D_c^t = 130$ m, LOS).

colors represent different materials, including metal, concrete, wood, and glass (not displayed). In the DR and GR models, the reflection coefficients are related to the material properties. The relevant parameters for these scenarios are given in Table III.

The simulation data are processed to obtain the PDP at $t = 0.1$ s and $f_c = 28$ GHz, as illustrated in Fig. 5. It is worth considering how to distinguish GR, DR, and other NLOS paths for RT. The machine-learning-based approach is mentioned in [54]. Another approach is to identify the path propagation mechanism of RT by angle and delay, and a idea of calibration is provided in [55]. The LOS, GR, DR, and other NLOS paths are distinguished according to the delay, angle, and reflective order of each path provided by RT in this paper. The results indicate that the DR components are existed in above three the industrial environments.

We have already performed the relevant measurement for the IIoT scenario, and the details are described in [56]. The fitted cumulative distribution functions (CDFs) of RMS azimuth spread of arrival(ASA) and RMS DS for the IIoT scenario are shown in Fig. 6 and Fig. 7, respectively. 3GPP [43] is the reference model, but the DR components proposed in this paper are not considered. The results show that the sim-

ulations are well-matched to the measurements. The accuracy of the proposed model is confirmed from time domain and angle domain.

What's more, RT simulation is performed to verify the generality of the proposed model at mmWave bands. The automated workshop, laboratory, and warehouse are the typical examples of IIoT scenarios. The fitted CDFs of RMS DS for the IIoT scenarios are shown in Fig 8. The results show that the proposed model provide a better fit for RT simulation compared with the 3GPP model without DR components at mmWave bands. This suggests that considering the DR components can provide a more accurate description of the industrial channel characteristics. In addition, the fitting results of multiple scenarios verify that the proposed model is general.

Fig. 9 displays the characteristics of DR components in industrial environments by presenting the power ratio of DR components for different antenna heights and K_{LOS} factors. It is assumed that Tx and Rx are at the same height from the ground, and the height relative to the ground is defined as Δh . The different values of K_{LOS} simulate different LOS scenarios, such as LOS with a light surrounding clutter (LOS-L) and LOS with a heavy surrounding clutter (LOS-H). The greater the clutter density of the environment is, the smaller

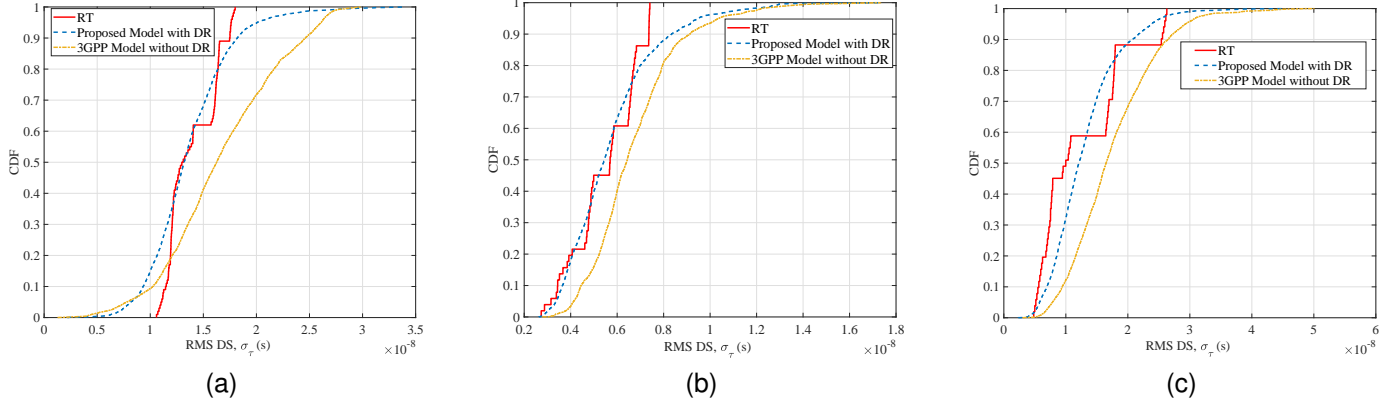


Fig. 8. Comparison of the RT modeled and simulated CDFs of RMS DS: (a) Automatic Workshop, (b) Lab, and (c) Warehouse ((a) $f_c = 28$ GHz, $\|\mathbf{D}\| = 15$ m, $M_R = M_T = 1$, $h_{rx,q} = 0.5$ m, $h_{tx,p} = 1$ m, $d_{1,q} = d_{1,p} = 1$ m, $d_{2,q} = d_{2,p} = 3$ m, $d_{l,qp} = d_{2D,qp} = 15$ m, $v^T = 0.5$ m/s, $v^R = 0$ m/s, $v^C = 0.2$ m/s, $D_c^s = 10$ m, $D_c^t = 130$ m, (b) $f_c = 28$ GHz, $\|\mathbf{D}\| = 3$ m, $M_R = M_T = 1$, $h_{rx,q} = 1$ m, $h_{tx,p} = 0.5$ m, $d_{1,q} = d_{1,p} = 1.5$ m, $d_{2,q} = d_{2,p} = 2.5$ m, $d_{l,qp} = d_{2D,qp} = 3$ m, $v^T = 0.5$ m/s, $v^R = 0$ m/s, $v^C = 0.2$ m/s, $D_c^s = 10$ m, $D_c^t = 130$ m, and (c) $f_c = 30$ GHz, $\|\mathbf{D}\| = 21$ m, $M_R = M_T = 1$, $h_{rx,q} = 2.5$ m, $h_{tx,p} = 2.5$ m, $d_{1,q} = d_{1,p} = 2.5$ m, $d_{2,q} = d_{2,p} = 3.5$ m, $d_{l,qp} = d_{2D,qp} = 21$ m, $v^T = 0.5$ m/s, $v^R = 0$ m/s, $v^C = 0.2$ m/s, $D_c^s = 10$ m, $D_c^t = 120$ m).

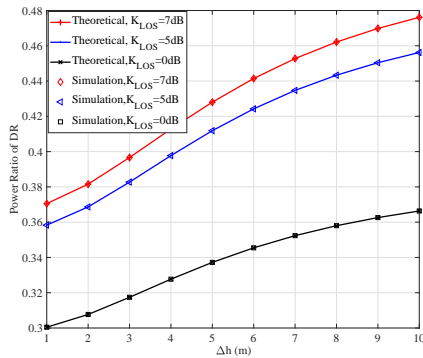


Fig. 9. Comparison of power ratio of DR components with different K_{LOS} factors ($f_c = 28$ GHz, $M_R = 16$, $M_T = 8$, $d_{1,q} = d_{1,p} = 1$ m, $d_{2,q} = d_{2,p} = 3$ m, $d_{l,qp} = d_{2D,qp} = 10$ m, $v^T = 0.5$ m/s, $v^R = 0$ m/s, $v^C = 0.2$ m/s, $D_c^s = 30$ m, $D_c^t = 130$ m).

value of K_{LOS} is. The results reveal that the percentage of the DR components increase with the antenna height. This is because the total power in (39) decreases with Δh under the influence of antenna height only, while the power of DR components is less affected by Δh . In addition, the percentage of DR components is proportional to K_{LOS} , i.e., the percentage of DR components in the LOS-L scenario is larger than that of the LOS-H scenario. What's more, the theoretical values are compared with the simulated values to verify that the trend highlighted is general. The results show that the theoretical results agree well with the simulations. It is worth noting that the theoretical values represent the calculated result of (40), and the simulations represent the calculated result of substituting the power of each component into (39).

To verify the accuracy of the proposed model regarding the number of scatters, the CDFs of the inter-cluster delay are examined, as shown in Fig. 10. The measurements from [38],

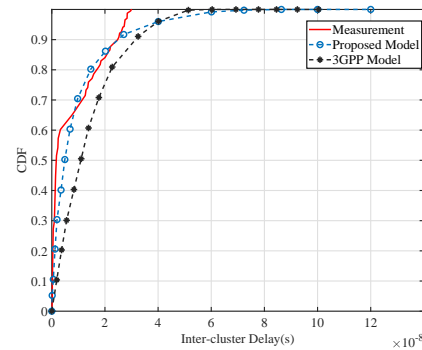


Fig. 10. Comparison of the measured and simulated CDFs of inter-cluster delay ($f_c = 60$ GHz, $\mathbf{D} = [20 \ -5 \ 0]$ m, $M_R = M_T = 32$, $D_c^s = 132$ m, $k_e = 0.39$, $\sigma_e = 1.14$, $\mu_e = 1.64$, $k_p = -0.12$, $\sigma_p = 2.32$, and $\mu_p = 1$).

and 3GPP channel model [37] are used for comparison. It is worth noting that 3GPP model utilizes Poisson distribution to simulate the number of clusters and rays. The root-mean-square error (RMSE) is used as the statistical measure. The RMSE of the fitting between the proposed model and the measurements is 0.0596. The RMSE of the fitting between the 3GPP model and the measurements is 0.1751. The results show that the proposed model is more accurate than the traditional distribution, since the signal is more sensitive to obstacles during the transmission process at mmWave bands, and the scatters are dense and random in complex industrial environments.

In this paper, RT simulations are used to verify the validity of the proposed Doppler shift model in industrial environments, and the results are shown in Fig. 11. The results show that the Doppler shift in the automatic workshop fit well with the Gaussian distribution, with the mean value of 26.75 and standard deviation of 15.0618. The RMSE of the fitting between the model and RT is 0.0314. Consequently, it is necessary to include random Doppler offset following

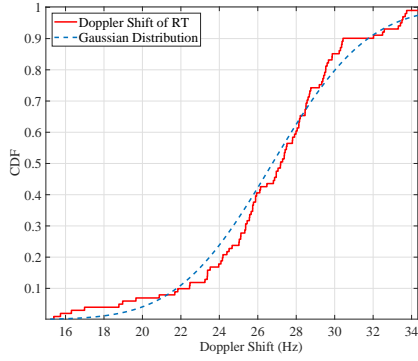


Fig. 11. Fitting results of the Doppler shift ($f_c = 28$ GHz, $M_R = M_T = 1$, $v^T = 0.5$ m/s, $v^R = 0$ m/s, $v^C = 0.2$ m/s, and Gaussian distribution with the mean value of 26.75 and standard deviation of 15.0618).

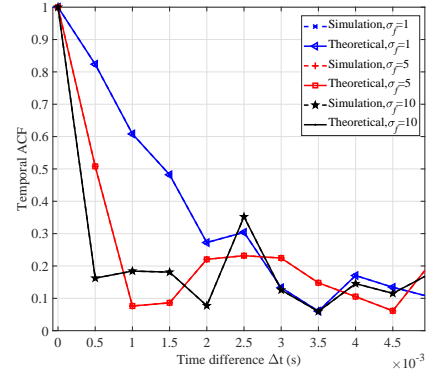


Fig. 12. Comparison between the normalized analytical and simulated temporal ACFs with different σ_f of Doppler random frequency offset ($f_c = 28$ GHz, $M_R = M_T = 2$, $d_{2D,qp} = 50$ m, $v^T = 0.5$ m/s, $v^R = v^C = 0.2$ m/s, $D_c^s = 30$ m, $D_c^t = 100$ m, NLOS).

Gaussian distribution in the proposed model.

The simulation results of the temporal ACF are shown in Fig. 12, where it can be seen that the simulation model matches well with the theoretical model, which prove the accuracy of the proposed STFCF model. Furthermore, the trend of ACFs are tested under different variance values σ_f , where the value of variance indicates the intensity of equipment's oscillation in industrial environments. According to the results, the larger σ_f leads to the smaller temporal ACF. This may be because the violent oscillations of the machines can cause the larger fluctuations of signal, which reduces the temporal ACF.

The simulation results of the space CCF are presented in Fig. 13, where it can be observed that the value of space CCF decreases with the antenna spacing. This could be explained by the spatial non-stationary characteristic caused by the massive MIMO. In addition, the space CCFs with the different $\eta(t)$ at time t are compared and analyzed. The results demonstrate that the larger power ratio of DR components leads to the smaller value of space CCF. This is because the larger power ratio of the DR components indicates the larger envelope fluctuations of signal, resulting in the smaller value of space CCF.

For the $M_R \times M_T$ communication system, $N(t) = N$, $M_n(t) = M_n$ and $L(t) = L$ are assumed at time t for simplicity. $20 + (10NM_n + 6N + L + 1)M_R M_T + (L + 1)(M_R + M_T)$ parameters are required to construct the CIR of the proposed model. Compared to the proposed model, $17 + M_R + M_T + (10N + 10NM_n + 1)M_R M_T$ parameters are required for construction in 3GPP.

For the deterministic models, $2NM_n M_R M_T$ parameters are required to build its CIR. The CIR is expressed as

$$h_{qp}(t) = \sum_{n=1}^N \sum_{m_n}^{M_n} a_{n,m_n} \delta(t - \tau_{n,m_n}) \quad (51)$$

where a_{n,m_n} and τ_{n,m_n} represent the amplitude and delay of the m th path within the n th cluster, respectively.

For the statistical models, $3NM_n M_R M_T$ parameters are required to build its CIR. The CIR is expressed as

$$h_{qp}(t) = \sum_{n=1}^N \sum_{m_n=1}^{M_n} a_{n,m_n} e^{j\theta_{n,m_n}} \delta(t - \tau_{n,m_n}) \quad (52)$$

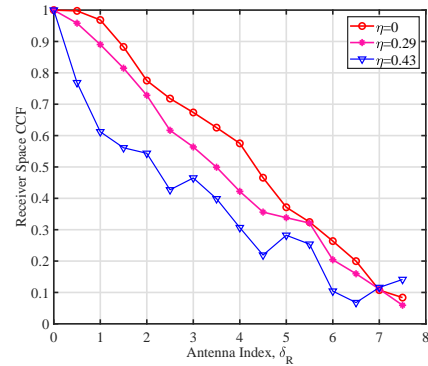


Fig. 13. Comparison between the normalized space CCFs with different power ratio r of DR components ($f_c = 28$ GHz, $M_R = 16$, $M_T = 1$, $d_{2D,qp} = 10$ m, $v^R = 1$ m/s, $v^T = 0$ m/s, $v^C = 0.5$ m/s, $D_c^s = 1$ m, $D_c^t = 100$ m).

where θ_{n,m_n} represents the phase shift of the m th path within the n th cluster. The computation overhead of the above models is counted as shown in Table IV.

Although the computation overhead of deterministic or statistical model is smaller than that the proposed model, its accuracy depends on a high precision description of the environment or extensive measurement activities. In addition, the computation overhead needs to be sacrificed to improve the accuracy of the proposed model.

VI. CONCLUSIONS

This paper has presented a 3D non-stationary GBSM for B5G IIoT, where DR components have been constructed according to the geometrical optics theory. The numbers of clusters and rays within a cluster in B5G IIoT scenarios have been modeled using the GEV and GP distributions. The Gaussian distribution has been combined with the traditional Doppler shift to establish the modified Doppler shift for the IIoT channel. The key channel statistical properties have been discussed and analyzed to verify accuracy and validity of the proposed model, including PDP, RMS DS, RMS AS, inter-cluster delay, Doppler shift, and STFCF. Combined with RT simulations, the results of PDP, RMS DS, RMS AS, and

TABLE IV
COMPUTATION OVERHEAD.

Model	Number of parameters
Proposed Model	$20 + (10NM_n + 6N + 1 + L)M_R M_T + (L + 1)(M_R + M_T)$
3GPP Model	$17 + (10NM_n + 10N + 1)M_R M_T + M_R + M_T$
Deterministic Model	$2NM_n M_R M_T$
Statistical Model	$3NM_n M_R M_T$

TABLE V
MATERIAL PROPERTIES

Material Type	Relative Permittivity		Conductivity (S/m)		Frequency Range (GHz)
	a_ϵ	b_ϵ	c_σ	d_σ	
Metal	1	0	10^7	0	1–100
Concrete	5.31	0	0.0326	0.8095	1–100
Wood	1.99	0	0.0047	1.0718	1–100
Glass	6.27	0	0.0043	1.1925	1–100

Doppler shift indicate the accuracy of the proposed model. The fitting results between the simulated and the measurement on inter-cluster delay reflect the good performance of the proposed model. The study demonstrates that the percentage of DR components is inversely proportional to the antenna height, and the percentage of DR components in LOS-H scenario is higher than that in LOS-L scenario. Furthermore, the simulated temporal ACFs and space CCFs describe the correlation of the proposed model at time and space domains, respectively. The above results reveal that the proposed model can support uRLLC and mMTC for IIoT communication systems.

However, there is a lack of more convincing measurements to support this model. Therefore the future work could further validate the accuracy of the proposed IIoT GBSM with more available channel measurements. Moreover, the proposed IIoT GBSM can be expanded to the the 6G channel modeling given the space-time-frequency consistency of industrial channels.

APPENDIX

REFLECTION COEFFICIENTS CALCULATION

The reflection coefficients of the parallel and vertical polarizations for the DR components in the proposed model can be respectively expressed as [57]

$$R_{\parallel}^{DR_i}(t) = \frac{\frac{\epsilon_{DR_i}}{\epsilon_0} \cos \varphi_{DR_i}^{EOD}(t) + \sqrt{\frac{\epsilon_{DR_i}}{\epsilon_0} - \sin^2(\varphi_{DR_i}^{EOD}(t))}}{\frac{\epsilon_{DR_i}}{\epsilon_0} \cos \varphi_{DR_i}^{EOD}(t) - \sqrt{\frac{\epsilon_{DR_i}}{\epsilon_0} - \sin^2(\varphi_{DR_i}^{EOD}(t))}} \quad (53)$$

$$R_{\perp}^{DR_i}(t) = \frac{\cos \varphi_{DR_i}^{EOD}(t) + \sqrt{\frac{\epsilon_{DR_i}}{\epsilon_0} - \sin^2(\varphi_{DR_i}^{EOD}(t))}}{\cos \varphi_{DR_i}^{EOD}(t) - \sqrt{\frac{\epsilon_{DR_i}}{\epsilon_0} - \sin^2(\varphi_{DR_i}^{EOD}(t))}} \quad (54)$$

In the above equation, the complex relative dielectric constant of a material is calculated as

$$\frac{\epsilon_{DR_i}}{\epsilon_0} = \epsilon_r - j \frac{\sigma}{2\pi f_c \epsilon_0} \quad (55)$$

where the electric constant is $8.854187817 \dots \times 10^{-12} \text{ F} \cdot \text{m}^{-1}$.

In a wireless propagation scenario, the values of relative dielectric constant ϵ_r and electrical conductivity σ are both

frequency-dependent parameters [58], and they can be respectively expressed as

$$\epsilon_r = a_\epsilon \cdot \left(\frac{f_c}{10^9} \right)^{b_\epsilon} \quad (56)$$

$$\sigma = c_\sigma \cdot \left(\frac{f_c}{10^9} \right)^{d_\sigma} \quad (57)$$

The relevant parameters of ϵ_r and σ can be found in [59]. Relevant parameters of the material from 1 GHz to 100 GHz are presented in Table V. Similarly, the reflection coefficients of the parallel and vertical polarizations for the GR components can be calculated.

REFERENCES

- [1] C.-X. Wang, X. You, X. Gao, *et al.*, "On the road to 6G: Visions, requirements, key technologies and testbeds," *IEEE Commun. Surveys Tuts.*, vol. 25, no. 2, pp. 905–974, Feb. 2023.
- [2] C.-X. Wang, J. Huang, H. Wang, *et al.*, "6G wireless channel measurements and models: Trends and challenges," *IEEE Veh. Technol. Mag.*, vol. 15, no. 4, pp. 22–32, Dec. 2020.
- [3] X. You, C.-X. Wang, J. Huang, *et al.*, "Towards 6G wireless communication networks: Vision, enabling technologies, and new paradigm shifts," *Sci. China Inf. Sci.*, vol. 64, no. 1, pp. 1–74, Jan. 2021.
- [4] T. S. Rappaport and C. D. McGillem, "UHF multipath and propagation," in *Proc. IEEE GLOBECOM*, Hollywood, USA, Nov. 1988, pp. 825–831.
- [5] T. S. Rappaport, "Delay spread and time delay jitter for the UHF factory multipath channel," in *Proc. IEEE VTC*, Philadelphia, USA, Jun. 1988, pp. 186–189.
- [6] D. He, B. Ai, K. Guan, *et al.*, "The design and applications of high-performance ray-tracing simulation platform for 5G and beyond wireless communications: A tutorial," *IEEE Commun. Surv. Tut.*, vol. 21, no. 1, pp. 10–27, 2019.
- [7] A. A. M. Saleh and R. A. Valenzuela, "A statistical model for indoor multipath propagation," *IEEE J. Sel. Areas Commun.*, vol. 5, no. 2, pp. 128–137, Feb. 1987.
- [8] U. T. Virk, K. Haneda, and J.-F. Wagen, "Dense multipath components add-on for COST 2100 channel model," in *Proc. IEEE EuCAP*, Lisbon, Portugal, Apr. 2015, pp. 1–5.
- [9] W. Hou, B. Du, Q. Wang, *et al.*, "Simulations and analysis for radio wave propagation properties in 5G frequency band in an industrial environment," in *Proc. IEEE IAEAC*, Chongqing, China, Mar. 2021, pp. 1019–1023.
- [10] T. Jiang, L. Tian, J. Zhang, *et al.*, "The impact of antenna height on the channel model in indoor industrial scenario," in *Proc. IEEE ICC Workshops*, Chongqing, China, Aug. 2020, pp. 1–6.

- [11] K. Zhang, L. Liu, C. Tao, *et al.*, "Doppler frequency trajectories of the mechanical robot arm and automated guided vehicle in industrial scenarios," in *Proc. IEEE VTC*, Kuala Lumpur, Malaysia, Apr. 2019, pp. 1–5.
- [12] M. F. Iskander and Z.-Q. Yun, "Propagation prediction models for wireless communication systems," *IEEE Trans. Microw. Theory Tech.*, vol. 50, no. 3, pp. 662–673, Mar. 2002.
- [13] I. P. Guembe, P. Lopez-Iturri, H. Klaina, *et al.*, "Wireless characterization and assessment of an UWB-based system in industrial environments," *IEEE Access*, vol. 9, pp. 107824–107841, Jul. 2021.
- [14] L. Wang, B. Ai, D. He, *et al.*, "Channel characteristics analysis in smart warehouse scenario," in *Proc. IEEE APS/URSI*, San Diego, USA, Jul. 2017, pp. 1417–1418.
- [15] D. Solomitskii, A. Orsino, S. Andreev, *et al.*, "Characterization of mmWave channel properties at 28 and 60 GHz in factory automation deployments," in *Proc. IEEE WCNC*, Barcelona, Spain, Apr. 2018, pp. 1–6.
- [16] J. Yang, B. Ai, I. You, *et al.*, "Ultra-reliable communications for industrial Internet of things: Design considerations and channel modeling," *IEEE Netw.*, vol. 33, no. 4, pp. 104–111, Jul. 2019.
- [17] S. Shikhantsov, A. Thielens, G. Vermeeren, *et al.*, "Hybrid ray-tracing/FDTD method for human exposure evaluation of a massive MIMO technology in an industrial indoor environment," *IEEE Access*, vol. 7, pp. 21020–21031, Feb. 2019.
- [18] Q. Zhang, L. Guo, W. Hou, *et al.*, "Wireless channel modeling through automatic stereoscopic warehouse in industrial Internet," in *Proc. IEEE ICC*, Qingdao, China, Oct. 2017, pp. 1–5.
- [19] M. Cheffena, "Industrial indoor multipath propagation – A physical-statistical approach," in *Proc. IEEE PIMRC*, Washington, USA, Sep. 2014, pp. 68–72.
- [20] T. S. Rappaport, S. Y. Seidel, and K. Takamizawa, "Statistical channel impulse response models for factory and open plan building radio communicate system design," *IEEE Trans. Commun.*, vol. 39, no. 5, pp. 794–807, May 1991.
- [21] J. Karedal, S. Wyne, P. Almers, *et al.*, "Statistical analysis of the UWB channel in an industrial environment," in *Proc. IEEE VTC*, Los Angeles, USA, Sep. 2004, pp. 81–85.
- [22] M. A. Matin, K. A. Yasmeen, and M. A. M. Ali, "Statistical model for UWB channel in an industrial environment," in *Proc. IEEE ICMNT*, Nanjing, China, Apr. 2008, pp. 1015–1017.
- [23] T. S. Rappaport, "Indoor radio communications for factories of the future," *IEEE Commun. Mag.*, vol. 27, no. 5, pp. 15–24, May 1989.
- [24] T. S. Rappaport and C. D. McGillem, "UHF fading in factories," *IEEE J. Sel. Areas Commun.*, vol. 7, no. 1, pp. 40–48, Jan. 1989.
- [25] S. Jaeckel, N. Turay, L. Raschkowski, *et al.*, "Industrial indoor measurements from 2-6 GHz for the 3GPP-NR and QuaDRiGa channel model," in *Proc. IEEE VTC*, Honolulu, USA, Sept. 2019, pp. 1–7.
- [26] E. Tanghe, W. Joseph, L. Verloock, *et al.*, "The industrial indoor channel: Large-scale and temporal fading at 900, 2400, and 5200 MHz," *IEEE Trans. Wireless Commun.*, vol. 7, no. 7, pp. 2740–2751, Jul. 2008.
- [27] B. Holfeld, D. Wieruch, L. Raschkowski, *et al.*, "Radio channel characterization at 5.85 GHz for wireless M2M communication of industrial robots," in *Proc. IEEE WCNC*, Doha, Qatar, Apr. 2016, pp. 1–7.
- [28] J. Karedal, S. Wyne, P. Almers, *et al.*, "A measurement-based statistical model for industrial ultra-wideband channels," *IEEE Trans. Wireless Commun.*, vol. 6, no. 8, pp. 3028–3037, Aug. 2007.
- [29] T. Olofsson, A. Ahlén, and M. Gidlund, "Modeling of the fading statistics of wireless sensor network channels in industrial environments," *IEEE Trans. Signal Process.*, vol. 64, no. 12, pp. 3021–3034, Jun. 2016.
- [30] P. Agrawal, A. Ahlén, T. Olofsson, *et al.*, "Long term channel characterization for energy efficient transmission in industrial environments," *IEEE Trans. Commun.*, vol. 62, no. 8, pp. 3004–3014, Aug. 2014.
- [31] M. Eriksson and T. Olofsson, "On long-term statistical dependences in channel gains for fixed wireless links in factories," *IEEE Trans. Commun.*, vol. 64, no. 7, pp. 3078–3091, Jul. 2016.
- [32] Z. Kun, L. Liu, T. Cheng, *et al.*, "Channel measurement and characterization for Industrial Internet of Things," in *Proc. IEEE WCNC*, Marrakesh, Morocco, Apr. 2019, pp. 1–5.
- [33] L. Liu, K. Zhang, C. Tao, *et al.*, "Channel measurements and characterizations for automobile factory environments," in *Proc. IEEE ICACT*, Chuncheon, Korea, Feb. 2018, pp. 234–238.
- [34] A. Miaouidakis, A. Lekkas, G. Kalivas, *et al.*, "Radio channel characterization in industrial environments and spread spectrum modem performance," in *Proc. IEEE ETFA*, Catania, Italy, Sept. 2005, pp. 87–93.
- [35] W. Fan, I. Carton, J. Ø. Nielsen, *et al.*, "Measured wide-band characteristics of indoor channels at centimetric and millimetric bands," *EURASIP J. Wireless Commun. Netw.*, vol. 2016, no. 1, pp. 1–13, Feb. 2016.
- [36] M. Schmieder, F. Undi, M. Peter, *et al.*, "Directional wideband channel measurements at 28 GHz in an industrial environment," in *Proc. IEEE GLOBECOM*, Waikoloa, USA, Dec. 2019, pp. 1–6.
- [37] M. Schmieder, T. Eichler, S. Wittig, *et al.*, "Measurement and characterization of an indoor industrial environment at 3.7 and 28 GHz," in *Proc. IEEE EuCAP*, Copenhagen, Denmark, Mar. 2020, pp. 1–5.
- [38] C. Cano, G. H. Sim, A. Asadi, *et al.*, "A Channel measurement campaign for mmWave communication in industrial settings," *IEEE Trans. Wireless Commun.*, vol. 20, no. 1, pp. 299–315, Jan. 2021.
- [39] L. Liu, J. Poutanen, F. Quitin, *et al.*, "The COST 2100 MIMO channel model," *IEEE Wireless Commun.*, vol. 19, no. 6, pp. 92–99, Dec. 2012.
- [40] P. Kyösti, J. Meinilä, T. Jämsä, *et al.*, *WINNER II Channel Models*, IST-4-027756, WINNER II D1.1.2, v1.2, Apr. 2008. [Online]. Available: <http://www.ist-winner.org/WINNER2-Deliverables/D1.1.2v1.1.pdf>.
- [41] Preliminary Draft New Report ITU-R M. [IMT–2020. EVAL], Channel Model (Part), Version 1, document ITU–R R15–WP5D-170613–TD–0332, Jun. 2017.
- [42] S. Jaeckel, L. Raschkowski, K. Börner, *et al.*, "QuaDRiGa – Quasi deterministic radio channel generator, user manual and documentation," Fraunhofer Heinrich Hertz Institute, Tech. Rep. v2.4.0. 2020.
- [43] "Study on channel model for frequencies from 0.5 to 100 GHz, V16.0.0," 3GPP, Sophia Antipolis, France, Rep. TR 38.901, Oct. 2019.
- [44] J. Bian, C.-X. Wang, X. Gao, *et al.*, "A general 3D non-stationary wireless channel model for 5G and beyond," *IEEE Trans. Wireless Commun.*, vol. 20, no. 5, pp. 3211–3224, May 2021.
- [45] S. Wu, C. Wang, e. M. Aggoune, *et al.*, "A general 3-D non-stationary 5G wireless channel model," *IEEE Trans. Wireless Commun.*, vol. 66, no. 7, pp. 3065–3078, Jul. 2018.
- [46] Y. Li, C.-X. Wang, and Y. Liu, "A 3D non-stationary geometry-based stochastic model for industrial automation wireless communication systems," in *Proc. IEEE PIMRC*, Helsinki, Finland, Sept. 2021, pp. 916–921.
- [47] D. P. Gaillot, E. Tanghe, W. Joseph, *et al.*, "Polarization properties of specular and dense multipath components in a large industrial hall," in *Proc. IEEE URSI GASS*, Beijing, China, Aug. 2014, pp. 1–4.
- [48] Y. Liu, C.-X. Wang, R. Dai, *et al.*, "A general 3D geometry-based stochastic model for industrial IoT environments," in *Proc. IEEE GC Wkshps*, Taipei, China, Dec. 2020, pp. 1–6.
- [49] C.-X. Wang, Z. Lv, X. Gao, *et al.*, "Pervasive wireless channel modeling theory and applications to 6G GBSMs for all frequency bands and all scenarios," *IEEE Trans. Veh. Technol.*, vol. 71, no. 9, pp. 9159–9173, Sept. 2022.
- [50] S. Coles, *An introduction to statistical modeling of extreme values*, New York: Springer, 2001.
- [51] J. Pickands III, "Statistical inference using extreme order statistics," *Ann. Statist.*, vol. 3, no. 1, pp. 119–131, Jan. 1975.
- [52] M. Pätzold, *Mobile radio channels*, Wiley Publishing, 2012.
- [53] T. Zwick, C. Fischer, D. Didascalou, *et al.*, "A stochastic spatial channel model based on wave-propagation modeling," *IEEE J. Sel. Areas Commun.*, vol. 18, no. 1, pp. 6–15, Jan. 2000.
- [54] K. Mao, Q. Zhu, M. Song, *et al.*, "Machine-Learning-Based 3-D channel modeling for U2V mmWave communications," *IEEE Internet Things J.*, vol. 9, no. 18, pp. 17592–17607, Sept. 2022.
- [55] K. Guan, B. Peng, D. He, *et al.*, "Channel sounding and ray tracing for intrawagon scenario at mmWave and sub-mmWave bands," *IEEE T. Antenn. Propaga.*, vol. 69, no. 2, pp. 1007–1019, Feb. 2021.
- [56] L. Zhang, C.-X. Wang, Z. Zhou, *et al.*, "Wireless channel measurements and characterization in 6G industrial IoT scenarios," *IEEE Trans. Veh. Technol.*, to be submitted.
- [57] E. C. Jordan and K. G. Balmain, *Electromagnetic waves and radiating systems*, Prentice-Hall, 1968.
- [58] ITU-R Rec. P.2040-1, "Effects of building materials and structures on radiowave propagation above about 100 MHz," International Telecommunication Union Radiocommunication Sector ITU-R, 2015.
- [59] ITU-R Rec. P.527-3, "Electrical characteristics of the surface of the earth," International Telecommunication Union Radiocommunication Sector ITU-R, 1992.



Wen Gu was born in Fuyang, Anhui, China, in 1995. She received the B.S. degree from Huaibei Normal University, Huaibei, Anhui, China, in 2020. She is currently studying for the M.S. degree in the School of Internet of Things Engineering, Jiangnan University, Wuxi, Jiangsu, China. Her research interest includes wireless propagation and channel modeling.



Cheng-Xiang Wang (Fellow, IEEE) received the B.Sc. and M.Eng. degrees in communication and information systems from Shandong University, China, in 1997 and 2000, respectively, and the Ph.D. degree in wireless communications from Aalborg University, Denmark, in 2004.

He was a Research Assistant with the Hamburg University of Technology, Hamburg, Germany, from 2000 to 2001; a Visiting Researcher with Siemens AG Mobile Phones, Munich, Germany, in 2004; and a Research Fellow with the University of Agder, Grimstad, Norway, from 2001 to 2005. He has been with Heriot-Watt University, Edinburgh, U.K., since 2005, where he was promoted to a Professor in 2011. In 2018, he joined Southeast University, Nanjing, China, as a Professor. He is also a part-time Professor with Purple Mountain Laboratories, Nanjing. He has authored four books, three book chapters, and more than 500 papers in refereed journals and conference proceedings, including 27 highly cited papers. He has also delivered 24 invited keynote speeches/talks and ten tutorials in international conferences. His current research interests include wireless channel measurements and modeling, 6G wireless communication networks, and electromagnetic information theory.

Dr. Wang is a member of the Academia Europaea (The Academy of Europe) and the European Academy of Sciences and Arts (EASA); a fellow of the Royal Society of Edinburgh (FRSE), IET, and China Institute of Communications (CIC); a Distinguished Lecturer of IEEE Communications Society in 2019 and 2020; and a Highly-Cited Researcher recognized by Clarivate Analytics from 2017 to 2020. He is currently an Executive Editorial Committee Member of the IEEE Transactions on Wireless Communications. He has served as a TPC Member, the TPC chair, and the general chair for more than 80 international conferences. He received 14 Best Paper Awards from IEEE GLOBECOM 2010, IEEE ICCT 2011, ITST 2012, IEEE VTC 2013 Spring, IWCMC 2015, IWCMC 2016, IEEE/CIC ICC 2016, WPMC 2016, WOCC 2019, IWCMC 2020, WCSP 2020, CSPS 2021, and WCSP 2021. He received the 2020–2022 “AI 2000 Most Influential Scholar Award Honorable Mention” in recognition of his outstanding and vibrant contributions in the field of the Internet of Things. He served as an Editor for over ten international journals, including the IEEE Transactions on Wireless Communications from 2007 to 2009, the IEEE Transactions on Vehicular Technology from 2011 to 2017, and the IEEE Transactions on Communications from 2015 to 2017. He was a Lead Guest Editor for the Special Issue on Vehicular Communications and Networks and a Guest Editor for the Special Issue on the Spectrum and Energy Efficient Design of Wireless Communication Networks and the Special Issue on Airborne Communication Networks of the IEEE Journal on Selected Areas in Communications. He was also a Guest Editor for the Special Issue on Wireless Big Data of the IEEE Transactions on Big Data and is a Guest Editor for the Special Issue on Intelligent Resource Management for 5G and Beyond of the IEEE Transactions on Cognitive Communications and Networking.



Yang Liu (M'18) was born in Wuxi, Jiangsu, China, in 1988. He received the Ph.D. degree in communication and information system from Key Laboratory of Wireless Communication, Nanjing University of Posts and Telecommunications (NUPT), Nanjing, China, in 2016. He is currently an associate Professor in Institute of IOT Engineering, Jiangnan University, Wuxi, Jiangsu. He has authored and co-authored over 10 technical papers published in peer-reviewed international journals and conference proceedings. His research interests include the wireless channel modeling and network coding.



Wenchao Xu is a research assistant professor at The Hong Kong Polytechnic University. He received his Ph.D. degree from University of Waterloo, Canada, in 2018. Before that he received the B.E. and M.E. degrees from Zhejiang University, Hangzhou, China, in 2008 and 2011, respectively. In 2011, he joined Alcatel Lucent Shanghai Bell Co. Ltd., where he was a Software Engineer for telecom virtualization. He has also been an Assistant Professor at School of Computing and Information Sciences in Caritas Institute of Higher Education, Hong Kong.

His research interests include wireless communication, Internet of things, distributed computing and AI enabled networking.



Yu Yu was born in Nanjing, China, in 1990. He received the B.E. and Ph.D. degrees in communication and information system from the Nanjing University of Posts and Telecommunications, Nanjing, in 2012 and 2017, respectively. He was a research engineer with Huawei Technologies Co., Ltd. He is currently a Lecturer with School of Information and Communication Engineering, Nanjing Institute of Technology, Nanjing. He has authored and co-authored over ten technical papers published in peer-reviewed international journals and conference

proceedings. His research interests include wireless propagation and wireless channel modeling.



Wen-Jun Lu (Senior Member) was born in Jiangmen, Guangdong, China, in 1978. He received Ph.D degree in electronic engineering from the Nanjing University of Posts and Telecommunications (NUP-T), Nanjing, China, in 2007. He has been a Professor with the Jiangsu Key Laboratory of Wireless Communications, NUPT, since 2013. His research interests include antenna theory, antenna design, antenna arrays, and wireless propagation channel modelling. From 2015 to 2016, he invented the design approach to planar endfire circularly polarized

antennas. Recently, he has advanced the generalized odd-even mode theory and established a unified theoretical framework for all resonant elementary antennas under multi-mode resonance. He is the translator of the Chinese version *The Art and Science of Ultrawideband Antennas* (by H. Schantz). He has authored three books, *Antennas: Concise Theory, Design and Applications* (in Chinese, 2014), its 2nd edition of *Concise Antennas* (in Chinese, 2020) and *Multi-mode Resonant Antennas: Theory, Design and Applications* (CRC Press, May 2022). He has authored or co-authored over 200 technical papers published in peer-reviewed international journals and conference proceedings. He is the inventor and co-inventor of 2 USA patents and over 40 Chinese patents. He was a recipient of the Exceptional Reviewers Award of the IEEE *TRANSACTIONS ON ANTENNAS AND PROPAGATION* in 2016, 2020 and 2021, and the Outstanding Reviewers Award of the AEU: *Int. J. of Electronics and Communications* in 2018. He has been serving as an Editorial Board Member of the *International Journal of RF and Microwave Computer-Aided Engineering* since 2014, and an Associate Editor of the *Electronics Letters* since 2019.



Hong-Bo Zhu was born in Yangzhou, China, in 1956. He is currently the standing Director of the Chinese Institute of Electronics and the Director of the Jiangsu Key Laboratory of Wireless Communications, Nanjing University of Posts and Telecommunications. He has authored and co-authored over 100 journal papers and over 60 invention patents authorized. In the past five years, he has undertaken over 30 projects at the national, provincial and ministerial level. His research interests include wireless communications, Internet of Things, and EMC.